

# Universality of optical absorptance quantization in two-dimensional group-IV, III-V, II-VI, and IV-VI semiconductors

Michel Lannoo,<sup>1</sup> P. Tim Prins,<sup>2</sup> Zeger Hens,<sup>3</sup> Daniel Vanmaekelbergh,<sup>2</sup> and Christophe Delerue<sup>4,\*</sup>

<sup>1</sup>*Aix Marseille Université, CNRS, Université de Toulon, IM2NP UMR 7334, 13397, Marseille, France*

<sup>2</sup>*Debye Institute for Nanomaterials Science, University of Utrecht, Princetonplein 1, 3584 CC Utrecht, The Netherlands*

<sup>3</sup>*Physics and Chemistry of Nanostructures (PCN), Ghent University, 9000 Gent, Belgium*

<sup>4</sup>*Université de Lille, CNRS, Centrale Lille, Université Polytechnique Hauts-de-France, Junia, UMR 8520 - IEMN, F-59000 Lille, France*



(Received 28 October 2021; revised 25 December 2021; accepted 5 January 2022; published 19 January 2022)

The optical absorptance of a single graphene layer over a wide range of wavelengths is known to be remarkably constant at the universal value  $\pi\alpha$  where  $\alpha$  is the fine structure constant. Using atomistic tight-binding calculations, we show that the absorptance spectra of nanometer-thin layers (quantum wells) of group-IV, III-V, II-VI, or IV-VI semiconductors are characterized by marked plateaus at integer values of  $\pi\alpha$ , in the absence of excitonic effects. In the case of InAs, the results obtained are in excellent agreement with the currently available experimental data. By revisiting experimental data on semiconductor superlattices, we show that  $\pi\alpha$  is also a metric of their absorption when normalized to a single period. We conclude that the  $\pi\alpha$  quantization is universal in semiconductor quantum wells provided that excitonic effects are weak and is therefore not specific to the zero-gap graphene case. The physical origin of this universality and its limits are discussed using analytical models that capture the main underlying physics of the lowest optical transitions in III-V and II-VI semiconductor quantum wells. These models show that the absorptance is ruled by  $\pi\alpha$  independent of the material characteristics because of the presence of a dominant term in the Hamiltonian, linear in the wave vector  $\mathbf{k}$  ( $\sim \mathbf{V} \cdot \mathbf{k}$ ), which couples the conduction band to the valence bands. However, the prefactor in front of  $\pi\alpha$  is not unity as in graphene due to the different nature of the electronic states. In particular, the spin-orbit coupling plays an important role in bringing the absorptance plateaus closer to integer values of  $\pi\alpha$ . The case of IV-VI semiconductor (PbSe) quantum wells characterized by a rocksalt lattice and multivalley physics is very similar to that of graphene, with the specification that a “massful gap” is formed around the Dirac points.

DOI: [10.1103/PhysRevB.105.035421](https://doi.org/10.1103/PhysRevB.105.035421)

## I. INTRODUCTION

The fine structure constant  $\alpha$ , introduced by Arnold Sommerfeld [1], characterizes the strength of the interactions between charged particles and the electromagnetic field [2]. In condensed matter physics, this constant quantifies the response to electromagnetic excitation of a large number of very different systems, such as materials with topological phases [3] including the quantum Hall effect [4], graphene [5–10], black phosphorus multilayers [11], or plasmonic networks [12]. In particular, if an undoped graphene monolayer is irradiated, the amount of absorbed light in a wide range of wavelengths is given by the universal constant  $\pi\alpha \approx 2.3\%$ . Remarkably, this same value appears in the quantization of optical absorption through InAs nanometer thick layers (hereinafter referred to as quantum wells) [13]. In this case, after correction of local-field effects, the absorptance spectrum is characterized by a succession of several plateaus whose respective heights are very close to  $\pi\alpha$ . Surprisingly, however, the case of quantum wells of semiconductors other than InAs has not been studied so far.

This quantization is not universal. For example, ultrafine monolayers obtained by exfoliation of van der Waals materials, such as transition metal dichalcogenides, often show spectra of great richness, with bound exciton absorptances much higher than  $\pi\alpha$ , especially under the action of strong excitonic effects [14–19]. These effects are also very strong in ultrathin ( $\lesssim 2$  nm) layers of semiconductors synthesized by colloidal chemistry, often called nanoplatelets [20,20,21].

These observations have inspired theoretical attempts to identify the origin of the  $\pi\alpha$  quantization and its intrinsic limits [22–28]. In the case of graphene, deviations from  $\pi\alpha$  appear when electrons lose their Dirac fermion character as a nonzero mass, for example at high energy relative to the Dirac point [26–28]. The same effect appears when a gap is opened at the Dirac point, for example under the action of spin-orbit coupling (SOC), as predicted in the case of silicene, germanene, and stanene [25], and as shown in Sect. S8 of the Supplemental Material [29] (see also Refs. [30–33] therein).

All previous theoretical studies [22–28] were based on two-band models from which it was concluded that the  $\pi\alpha$  quantization of the absorptance results from a numerical compensation between the joint density-of-states (JDOS) and the oscillator strength. However, this cancellation of terms is only perfect in the case of pristine graphene, for which the Fermi velocity determines both the band dispersion and the

\*christophe.delerue@iemn.fr

TABLE I. Summary of the results for the different types of materials considered in this work. CB and VB stand for conduction and valence bands, respectively. The number of bands per valley must be multiplied by two if spin is taken into account. In the case of Ge, we consider the direct bands at  $\Gamma$ . The integer  $n > 0$  indicates that the absorptance present several plateaus, multiple of  $\pi\alpha$  or  $2\pi\alpha$ .

Material	Lattice	Valleys	Number of bands per valley	Band dispersion	SOC	Absorptance plateaus	Unit per valley
Graphene	Honeycomb	K ( $\times 2$ )	CB:1 VB:1	Linear	No	$\pi\alpha$	$\pi\alpha/2$
III-V or II-VI semiconductor	Zinc-blende	$\Gamma(\times 1)$	CB:1 VB:3	CB: Parabolic at the edge, nonparabolic beyond	Yes, sets VB SOC splitting	$\sim n\pi\alpha$	$\sim \pi\alpha$
Ge	Diamond	$\Gamma(\times 1)$		VB: Complex, anisotropy, warping			
IV-VI semiconductor	Rocksalt	L ( $\times 4$ )	CB:1 VB:1	Parabolic at edges, almost linear beyond	Yes, opens the gap	$\sim 2n\pi\alpha$	$\sim \pi\alpha/2$

momentum matrix elements over a large energy range [5–10,28]. In the case of quantum wells of zinc-blende semiconductors which are characterized by heavy, light, and split-off hole bands with marked anisotropies that couple under the effect of the confinement, a two-band model is not justified [34]. Previous theoretical studies [13,23,24,26] assumed a constant JDOS, typical of two-dimensional (2D) materials with parabolic bands. In reality, however, InAs is characterized by marked nonparabolic effects due to a very strong coupling between valence and conduction bands [35–37]. As a result, the fundamental physical reasons for the  $\pi\alpha$  quantization of the absorptance in InAs quantum wells remains largely to be revealed and so does the universality of this characteristics. In this paper, we show that absorptance quantization can be found in 2D materials characterized by very different band structures, such as graphene, group-IV, III-V, and II-VI semiconductors, and even in IV-VI semiconductors with a rocksalt lattice.

In the following, we present detailed atomistic tight-binding calculations of electronic structures and absorptance spectra of semiconductor quantum wells. As summarized in Table I, we predict that, despite band structures of great variety and complexity, quantum wells of many semiconductors are characterized by simple absorptance spectra with marked plateaus, directly interpretable in terms of the universal constant  $\pi\alpha$ . We show that InAs is not a singular example but is on the contrary representative of other conventional semiconductors with weak excitonic effects, which is already the case for InAs layers thicker than 3 nm [13]. These predictions are reinforced by published absorption measurements in semiconductor superlattices whose results we revisit [23].

We show that this universality of the absorptance quantization has a common fundamental origin that we are able to reveal through simple analytical models. The nature of the electronic states involved in the optical transitions plays essentially only on the prefactor in front of  $\pi\alpha$ , which differs according to the categories of materials. This universal behavior thus provides simple rules for the design of photodetectors based on semiconductor quantum wells. It creates an unexpected bridge with the world of graphene, not by coincidence but due to very fundamental reasons. Finally, we remark that reports show that the fine structure constant also rules spontaneous emission and gain, a topic beyond the scope of the present work [23].

## II. METHODOLOGY

### A. Expression for the absorptance

The absorptance  $\mathcal{A}$  is the measure of the absorbed light flux, such that  $\mathcal{R} + \mathcal{A} + \mathcal{T} = 1$  where  $\mathcal{T}$  is the transmittance and  $\mathcal{R}$  is the reflectance. In the case of a single quantum well deposited on a transparent substrate, the absorptance at photon energy  $\hbar\omega$  can be written as

$$\mathcal{A}(\hbar\omega) = F^2 \mathcal{A}_0(\hbar\omega), \quad (1)$$

where  $F$  is equal to  $2/(n_s + 1)$  in which  $n_s$  is the refractive index of the substrate (assumed to be very thick). The prefactor  $F^2$ , which is a local-field factor, describes the fact that the quantum well experiences interfering incident and reflected electric fields. In the case of a sample irradiated perpendicularly, a quantum well being a quasi-2D system, the external electric field (plus its reflected component) is unscreened (for wavelength  $\gg$  thickness), the polarization charges being repelled at the edges.

The rate for an optical transition between a valence subband  $v$  and a conduction subband  $c$  at wave vector  $\mathbf{k}$  is determined by the oscillator strength  $f_{c,v}(\mathbf{k}) = (2/m_0) |\langle c, \mathbf{k} | \mathbf{p} \cdot \mathbf{e} | v, \mathbf{k} \rangle|^2 / [E_c(\mathbf{k}) - E_v(\mathbf{k})]$  where  $\mathbf{e}$  is the light polarization vector,  $\mathbf{p}$  is the momentum operator,  $m_0$  is the free electron mass, and  $E_c(\mathbf{k})$  [ $E_v(\mathbf{k})$ ] is the energy in the conduction [valence] subband. In the absence of excitonic effects, the bare absorptance of a quantum well is given by [38,39]

$$\mathcal{A}_0(\hbar\omega) = \frac{\pi \hbar e^2}{2m_0 c \epsilon_0 S} \sum_{c,v,\mathbf{k}} f_{c,v}(\mathbf{k}) \delta(\hbar\omega - E_c(\mathbf{k}) + E_v(\mathbf{k})), \quad (2)$$

where  $S$  is the area of the sample on which we apply periodic boundary conditions that define the components of  $\mathbf{k}$ . For numerical implementation, the number of  $\mathbf{k}$  vectors is increased until the results are converged, the Dirac delta function  $\delta(x)$  in Eq. (2) being replaced by a Gaussian function  $\exp[-x^2/(2\eta^2)]/(\eta\sqrt{2\pi})$  where  $\eta$  characterizes all sources of broadening. Unless otherwise specified,  $\eta$  is fixed at 10 meV.

### B. Tight-binding calculations of the absorptance

The electronic structure of (001) quantum wells is calculated using an atomistic tight-binding method. Each atom of the compound is described by a set of 20 atomic orbitals,

$sp^3d^5s^*$  for each spin degree of freedom where  $s^*$  represents a second  $s$  orbital. The dangling bonds at quantum well surfaces are saturated with pseudohydrogen atoms described by a single  $s$  orbital [38], except for PbSe for which it is not necessary [40]. The Hamiltonian matrix elements are restricted to the nearest-neighbor interactions and onsite terms. Spin-orbit coupling is included. We used the tight-binding model of Ref. [41] for InAs, Ref. [40] for PbSe, Ref. [42] for (zinc-blende) CdSe, Ref. [43] for GaAs, Ref. [44] for Ge, Ref. [45] for HgTe. We have verified that very similar results have been obtained with other sets of parameters for PbSe [46] and for Ge [47]. Following a well-established recipe for the description in tight binding of the optical properties of semiconductors [38,48], the momentum matrix elements are determined by those of the Hamiltonian  $\mathbf{H}(\mathbf{k})$ ,

$$\langle c, \mathbf{k} | \mathbf{p} \cdot \mathbf{e} | v, \mathbf{k} \rangle \rightarrow \frac{m_0}{\hbar} \langle c, \mathbf{k} | \nabla H(\mathbf{k}) \cdot \mathbf{e} | v, \mathbf{k} \rangle \quad (3)$$

in which the gradient of  $\mathbf{H}(\mathbf{k})$  is relative to  $\mathbf{k}$ .

### C. Condition for the existence of plateaus in the absorptance

It is interesting to consider the case where the system is isotropic, i.e., where all quantities depend only on  $k$ , the modulus of  $\mathbf{k}$ . As shown in Appendix A, and as already found by Huang *et al.* [28], the bare absorptance can be written from Eq. (A4) as

$$\mathcal{A}_0(\hbar\omega) = 2\pi\alpha \sum_{c,v} \frac{|\langle c, \mathbf{k} | \nabla H(\mathbf{k}) | v, \mathbf{k} \rangle|^2}{\partial |E_v(k) - E_c(k)|^2 / \partial (k^2)} \quad (4)$$

with  $k$  such that  $E_c(k) - E_v(k) = \hbar\omega$ .  $\nabla H$ , the gradient of the Hamiltonian with respect to  $k$ , comes from the expression of the momentum [Eq. (3)]. The numerator and denominator of Eq. (4) have thus the same unit, i.e., (energy.length)<sup>2</sup>. Within one constant, the inverse of the numerator is equal to the joint density of states divided by  $\hbar\omega$  (Appendix A).

Equation (4) shows that, for the absorptance to be constant, there must be compensation between the optical matrix element  $|\langle c, \mathbf{k} | \nabla H(\mathbf{k}) | v, \mathbf{k} \rangle|^2$  and the denominator. As we show in the following, this is likely to occur when a nondiagonal term of the Hamiltonian, linear in  $k$  ( $\sim \mathbf{V} \cdot \mathbf{k}$  where  $\mathbf{V}$  is a constant vector), coupling conduction and valence subbands, dominates. In this case, both the numerator and denominator are proportional to  $|\mathbf{V}|^2$  and  $\mathcal{A}_0(\hbar\omega)$  is a constant determined by the symmetry of the electronic states.

## III. RESULTS AND DISCUSSION

### A. InAs

Figure 1 presents the absorptance for InAs quantum wells. The results of the calculations are compared with the experimental data of Ref. [13]. We have adjusted the thickness of the quantum wells in order to obtain the correct optical threshold (gap) compared to experiments. A reduction in thickness of the order of 2 nm is needed (Fig. 1), which can be understood by band-bending effects which are well known in the case of InAs surfaces, due to the pinning of the Fermi level by surface states [49].

The agreement between theory and experiments in Fig. 1 is quite remarkable, showing that excitonic effects which are not

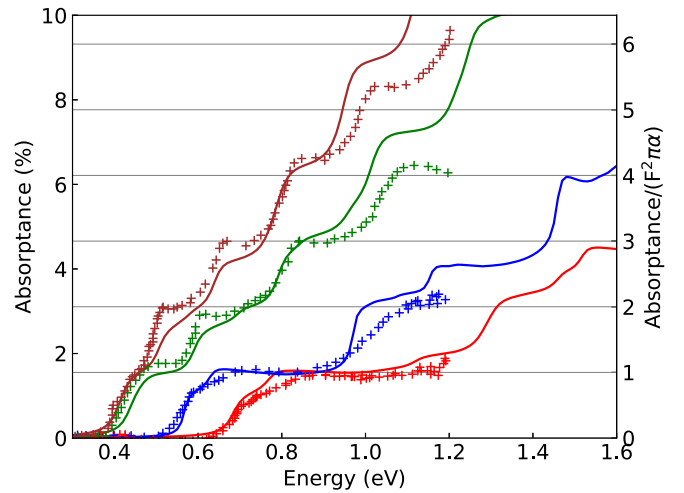


FIG. 1. Crosses: measured absorptance [13] for InAs quantum wells of different thickness, 6.0 nm (red), 9.0 nm (blue), 14 nm (green), 19 nm (brown). Solid lines: absorptance  $\mathcal{A}(\hbar\omega)$  calculated for quantum wells with slightly smaller thickness, 4.0 nm (red), 6.0 nm (blue), 12.5 nm (green), 17.5 nm (brown). Broadening:  $\eta = 20$  meV.

taken into account in our calculations are weak in these InAs quantum wells. The absorptance is characterized by very clear steps. Their position, their amplitude, and even their shape when they exhibit fine structures are well described by the calculations. The main plateaus in the spectra correspond to a  $\pi\alpha$  quantization of the bare absorptance  $\mathcal{A}_0(\hbar\omega)$ .

As shown in Fig. 2(a) for a 4 nm quantum well, the band structure is composed of subbands due to the vertical quantum confinement effect. The valence subbands [Fig. 2(b)] exhibit a complex dispersion, due to the contribution of the heavy-hole (HH), light-hole (LH), and split-off (SO) bands [34]. In spite of this complexity, the absorptance shown in Fig. 1 has relatively simple behavior, with main plateaus of  $\mathcal{A}_0(\hbar\omega)$  at  $n\pi\alpha$  with  $n \in \mathcal{N}$  (for additional results for a thickness of 12.5 nm, see Fig. S1 of Supplemental Material [29]).

Figure 2(c) presents the absorptance calculated using a smaller broadening to reveal the details. This shows that the first plateau is in fact composed of three steps corresponding to the transitions from valence subbands  $\text{HH}_1$ ,  $\text{LH}_1$ , and  $\text{SO}_1$  to the lowest conduction subband  $\text{CB}_1$  [Fig. 2(a) and Fig. 2(b)]. Here the index 1 represents the first quantum mode induced by the vertical confinement in the quantum well. Similarly, a detailed analysis shows that the plateau at  $n\pi\alpha$  can be associated with transitions  $(\text{HH}+\text{LH}+\text{SO})_n \rightarrow \text{CB}_n$  (Supplemental Material [29], Fig. S1 in Sec. S1).

It is important to point out that the description of the valence subbands in the form  $\text{HH}_n$ ,  $\text{LH}_n$ , and  $\text{SO}_n$  is only a simplified representation. Indeed, it is not easy to follow the HH, LH, SO character of the subbands as a function of  $k$  because of their nonparabolicity, their warping, and their  $k$ -dependent mixing under quantum confinement, which lead to complex dispersion including band crossings and anticrossings [Fig. 2(b)]. However, as shown in Appendix B and in the following sections, this simple representation is justified by extracting a 2D  $\mathbf{k} \cdot \mathbf{p}$  model from the atomistic tight-binding calculations. In other words, this very common description

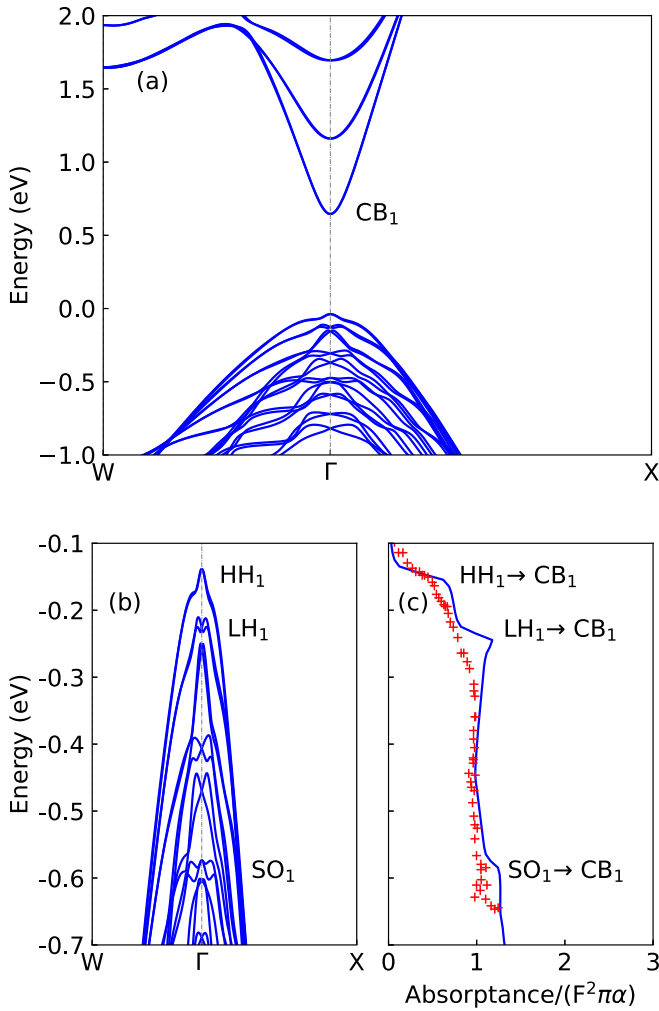


FIG. 2. (a) Lowest conduction subbands and highest valence subbands of a 4 nm thick InAs quantum well. (b) Zoom on the highest valence subbands and, facing each other, (c) plot of the bare absorbance calculated with a smaller broadening ( $\eta = 6$  meV) than in Fig. 1 in such a way that each absorbance plateau can be associated to a transition from a valence subband ( $HH_1$ ,  $LH_1$ ,  $SO_1$ ) to the lowest conduction subband ( $CB_1$ ). Red crosses: experiments [13] for a 6 nm thick quantum well. High symmetry points of the Brillouin zone:  $W = \pi/a[1, 1, 0]$ ,  $X = 2\pi/a[1, 0, 0]$ ,  $a$  being the bulk lattice parameter.

[34] of the bands in terms of HH, LH, and SO is well justified as long as we only want to describe the main optical transitions which tend to hide the subtle features of the band structure.

## B. Other semiconductors

InAs is a semiconductor characterized by a small band gap. It is therefore interesting to test the quantization of absorption in the case of semiconductors with a higher band gap. Figure 3 shows that the absorbance spectra of GaAs and CdSe quantum wells are also characterized by several well-marked steps close to multiples of  $\pi\alpha$ . The deviations from  $\pi\alpha$  are here larger than for InAs but remain relatively modest.

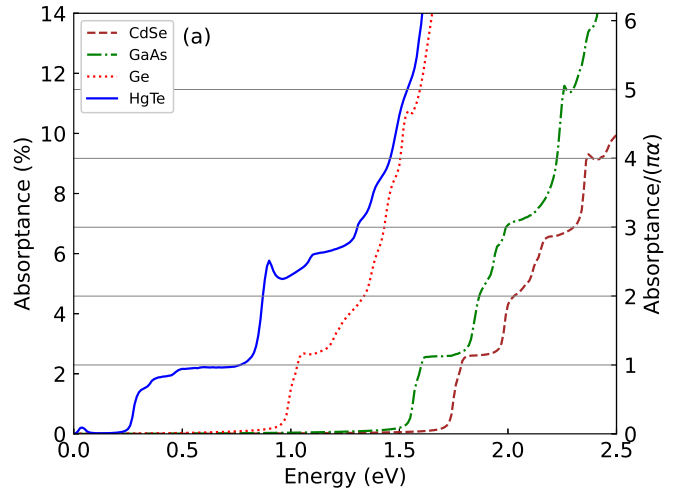


FIG. 3. Bare absorbance  $\mathcal{A}_0(\hbar\omega)$  calculated for 6 nm thick quantum wells of CdSe (brown dashed line), Ge (red dotted line), GaAs (green dotted-dashed line), and for a 3.9 nm thick quantum well of HgTe (blue solid line).

Remarkably, the first step of  $\mathcal{A}_0(\hbar\omega)$  at  $\approx \pi\alpha$  is also clearly visible in the case of a Ge quantum well, yet an indirect semiconductor. In fact, in bulk Ge, the minimum of the conduction band at  $\Gamma$  is just above the minima at L points, so the first step corresponds to the vertical transitions in the vicinity of  $\Gamma$ . At higher energy, the steps are less visible, due to the complex conduction band structure of Ge in this region [50].

Another particularly interesting system is HgTe, a semimetal, which can be seen as an inverted band semiconductor due to the strong SOC. Under the effect of a weak quantum confinement, a band gap opens, leading to the formation of a topological insulator as long as band remains inverted [51–53]. When the thickness of the layers is reduced, the band gap closes and then opens again. In this case, the band order of a conventional semiconductor is restored. Remarkably, a band gap of the order of one electron volt can even be obtained in ultrathin layers, colloidal nanoplatelets [54]. We have therefore considered a 3.9 nm thick (001) HgTe quantum well, characterized by a band gap of 0.19 eV, thin enough to be in the noninverted regime, thick enough to minimize the excitonic effects. Figure 3 shows that the absorbance spectrum is again characterized by a very marked plateau at  $\pi\alpha$ . However, this plateau is preceded by several intermediate steps, which are relatively long, but whose contributions converge towards  $\pi\alpha$ . These steps, as well as the sharp peaks visible at higher energy, are due to the complex energy dispersion of the valence subbands with heavy-hole and light-hole components (Supplemental Material [29], Fig. S2).

## C. Role of spin-orbit coupling

Figure 4 illustrates the effect of the SOC. In the absence of SOC,  $\mathcal{A}_0(\hbar\omega)$  in InAs and CdSe quantum wells is still quantized, but the height of the first plateau is closer to  $1.5\pi\alpha$  than  $\pi\alpha$ . This is also true for the following steps which are clearly larger than  $\pi\alpha$ . When the SOC is restored, the quantization in  $\pi\alpha$  becomes remarkable. In the following, in order

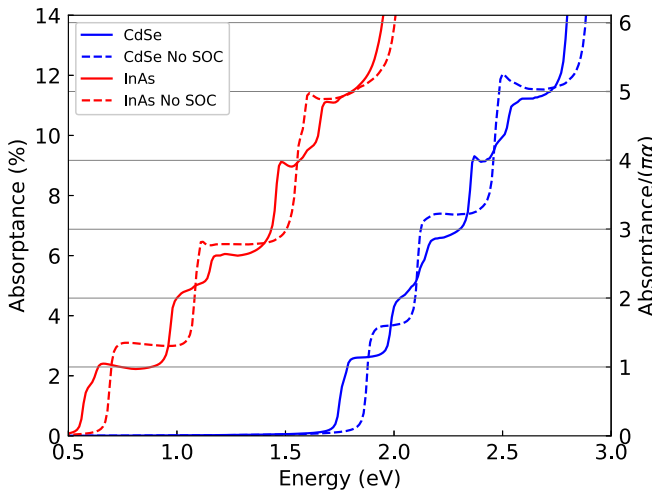


FIG. 4. Bare absorbance  $\mathcal{A}_0(\hbar\omega)$  calculated in tight binding for 6-nm-thick layers of InAs (red curves) or CdSe (blue curves), with (solid lines) or without (dashed lines) SOC.

to understand these behaviors, we will work in two steps, first, by proposing an analytical model of  $\mathcal{A}_0(\hbar\omega)$  in the absence of SOC, second, by understanding the effect of SOC on the absorbance step height.

#### IV. FUNDAMENTALS OF THE ABSORPTANCE PLATEAUS

##### A. The prototypical model of graphene

To illustrate the compensation mechanism in Eq. (4), it is interesting to return to the case of graphene to understand what is happening in semiconductor quantum wells. In each valley  $K$  or  $K'$  of graphene, the Hamiltonian matrix near the Dirac point (zero of energy) can be written, in the basis of the Bloch functions made of  $p_z$  orbitals on the two sublattices of the honeycomb, as follows [55]

$$H = \begin{bmatrix} 0 & V(k_x + ik_y) \\ V^*(k_x - ik_y) & 0 \end{bmatrix}, \quad (5)$$

where  $V = \hbar v_F$  is related to the Fermi velocity  $v_F$ .

By defining bottom ( $\Psi_-$ ) and top ( $\Psi_+$ ) band states, the numerator and the denominator of Eq. (4) are given by

$$|\langle \Psi_+ | \nabla H(\mathbf{k}) | \Psi_- \rangle|^2 = |V|^2 \quad (6)$$

$$\partial |E_+(k) - E_-(k)|^2 / \partial k^2 = 4|V|^2. \quad (7)$$

There is a total compensation between these two terms in Eq. (4), so that  $|V|^2$  disappear [28]. The bare absorbance per valley is therefore  $\mathcal{A}_0(\hbar\omega) = \pi\alpha/2$ , independent of  $V$  and any material characteristics [5–10]. This compensation is no longer effective in the case of massive Dirac bands (Sec. S8 in Supplemental Material [29] and Refs. [25–28]).

##### B. A prototypical analytical model for semiconductor quantum wells

In this section, we present a three-band model based on the Kane Hamiltonian [56] that provides the simplest description of the absorbance in III-V or II-VI semiconductor quantum

wells, in the absence of SOC.  $\mathcal{A}_0(\hbar\omega)$  is calculated analytically as the sum of two components, the first of which is equal to  $\pi\alpha$ , the second depends only on the quantum well gap energy and tends to zero at high energy. This model thus sheds light on the fundamental origins of the quantization of the absorbance and its relative invariance from one semiconductor to another.

The model Hamiltonian  $H$  is defined in a basis of three vectors, corresponding to the Bloch states at  $\mathbf{k} = 0$ , one of  $s$  character ( $|s\rangle$ ) for the conduction band, two of  $p$  character ( $|x\rangle, |y\rangle$ ) for valence bands, translating the 2D character of the system. Keeping only the principal coupling terms at the first-order in  $k$  ( $\propto P$ ), we write

$$H = \begin{bmatrix} E_g & iPk_x & iPk_y \\ -iPk_x & 0 & 0 \\ -iPk_y & 0 & 0 \end{bmatrix}, \quad (8)$$

where  $E_g$  is the energy gap of the quantum well. Introducing two vectors,

$$\begin{aligned} |p_{\parallel}\rangle &= \frac{k_x|x\rangle + k_y|y\rangle}{k}, \\ |p_{\perp}\rangle &= \frac{k_y|x\rangle - k_x|y\rangle}{k}, \end{aligned} \quad (9)$$

the Hamiltonian in the basis  $\{|s\rangle, |p_{\parallel}\rangle, |p_{\perp}\rangle\}$  becomes

$$H = \begin{bmatrix} E_g & iPk & 0 \\ -iPk & 0 & 0 \\ 0 & 0 & 0 \end{bmatrix}. \quad (10)$$

The solutions are  $|\Psi_{hh}\rangle = |p_{\perp}\rangle$  of energy  $E_{hh} = 0$  (flat band), and the states  $|\Psi_e\rangle$  and  $|\Psi_{lh}\rangle$  of energy

$$E_{lh}^e(k) = \left(\frac{E_g}{2}\right) \pm \sqrt{\left(\frac{E_g}{2}\right)^2 + P^2k^2}, \quad (11)$$

respectively.  $E_e(k)$  is the energy of the conduction subband.  $E_{hh}(k)$  and  $E_{lh}(k)$  are the energies of HH and LH subbands, respectively. Interestingly, the energy dispersions in this model are basically the same as for massive Dirac fermions.

The absorbance coming from transitions  $|\Psi_{hh}\rangle \rightarrow |\Psi_e\rangle$  and  $|\Psi_{lh}\rangle \rightarrow |\Psi_e\rangle$  is written as  $\mathcal{A}_0(\hbar\omega) = \mathcal{A}_{hh-e}(\hbar\omega) + \mathcal{A}_{lh-e}(\hbar\omega)$  and is calculated analytically using Eq. (4), replacing ( $|v, \mathbf{k}\rangle, |c, \mathbf{k}\rangle$ ) by ( $|\Psi_{hh}\rangle, |\Psi_e\rangle$ ) or ( $|\Psi_{lh}\rangle, |\Psi_e\rangle$ ), respectively. Details on the calculations are given in Supplemental Material [29], Sec. S4.

##### 1. Calculation of the absorbance for the heavy-hole electron transition

For the transition  $\Psi_{hh} \rightarrow \Psi_e$  at the energy  $\hbar\omega = E_e(k) - E_{hh}(k)$ , the optical matrix element is given by (Supplemental Material [29], Sec. S4.1)

$$|\langle \Psi_e | \nabla H(\mathbf{k}) | \Psi_{hh} \rangle|^2 = \frac{P^2 \hbar\omega}{2\hbar\omega - E_g} \quad (12)$$

and the denominator of Eq. (4) by

$$\frac{\partial |E_e(k) - E_{hh}(k)|^2}{\partial k^2} = \frac{2P^2 \hbar\omega}{2\hbar\omega - E_g}. \quad (13)$$

We deduce the absorbance

$$\mathcal{A}_{lh-e}(\hbar\omega) = \pi\alpha \theta(\hbar\omega - E_g), \quad (14)$$

where  $\theta(x)$  is the unit step function.

Remarkably, as in the case of graphene, there is a complete compensation between the different terms so that the absorbance is a constant, independent of  $P$ ,  $E_g$ , and  $\hbar\omega$ . This compensation takes place while the JDOS is not constant (Supplemental Material [29], Sec. S4.1), unlike the ideal case of 2D parabolic valence and conduction bands.

### 2. Calculation of the absorbance for the light-hole electron transition

For the transition  $\Psi_{lh} \rightarrow \Psi_e$  at the energy  $\hbar\omega = E_e(k) - E_{lh}(k)$ , the optical matrix element is given by (Supplemental Material [29], Sec. S4.2)

$$|\langle \Psi_e | \nabla H | \Psi_{lh} \rangle|^2 = \left( \frac{E_g P}{\hbar\omega} \right)^2 \quad (15)$$

and the denominator of Eq. (4) by

$$\partial |E_e(k) - E_{lh}(k)|^2 / \partial k^2 = 4P^2. \quad (16)$$

The absorbance is thus given by

$$\mathcal{A}_{lh-e}(\hbar\omega) = \frac{\pi\alpha}{2} \left( \frac{E_g}{\hbar\omega} \right)^2 \theta(\hbar\omega - E_g). \quad (17)$$

Also remarkably, this contribution does not depend on  $P$ , is equal to  $\pi\alpha/2$  when  $\hbar\omega = E_g$  and tends to 0 when  $\hbar\omega \gg E_g$ .

This is at variance with graphene where the transition between the two band gives a plateau at  $\pi\alpha/2$ . Note that, as in the case of graphene, the JDOS is proportional to  $\hbar\omega$  [Eq. (S32) in Supplemental Material [29]]. The difference is therefore due to different local 2D symmetries, i.e., to the different nature of the Bloch states.

### 3. Comparison to tight-binding calculations

The total absorbance in this simple model is therefore given by

$$\mathcal{A}_0(\hbar\omega) = \pi\alpha \left[ 1 + \frac{1}{2} \left( \frac{E_g}{\hbar\omega} \right)^2 \right] \theta(\hbar\omega - E_g). \quad (18)$$

Figure 5 shows that, despite its great simplicity, the analytical model reproduces remarkably well the results obtained by the tight-binding method, in the absence of SOC. This model describes the essential characteristics of the optical transitions from valence subbands to the first conduction subband. It gives a simple explanation to the quantization of the absorbance, and to its universal character since the Eq. (18) only involves the energy gap as a characteristic quantity of the semiconductor quantum well. As in the case of graphene,  $\pi\alpha$  is a metric of the absorbance.

### 4. Justification of the simple analytical model

We have shown in the previous sections that the valence band structure of III-V or II-VI semiconductor quantum wells is in general of great complexity. In this context, it is not

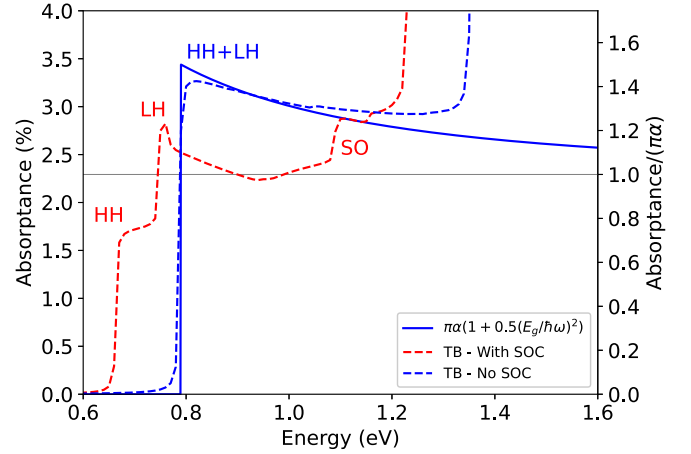


FIG. 5. Bare absorbance  $\mathcal{A}_0(\hbar\omega)$  for 4.2-nm-thick layer of InAs calculated in tight-binding (TB, dashed curves) with (red) or without (blue) SOC. The blue solid line shows  $\mathcal{A}_0(\hbar\omega)$  given by the simple analytical model, Eq. (18) with  $E_g = 0.79$  eV. For the sake of comparison, the tight-binding calculations were performed with a small broadening  $\eta$  of 2 meV.

obvious that a three-band model, including one flat band and two fully symmetric bands is representative of real systems.

The general justification of a 2D  $\mathbf{k} \cdot \mathbf{p}$  model, starting from a bulk Kane Hamiltonian, is presented in Supplemental Material [29], Sec. S3. We also present and justify in Appendix B a more elaborate ( $3 \times 3$ ) 2D  $\mathbf{k} \cdot \mathbf{p}$  model whose parameters are directly deduced from tight binding calculations, following the methodology described in Supplemental Material [29], Sec. S5. This model includes all matrix elements up to the second order in components of  $\mathbf{k}$ . We deduce from Appendix B that the simple analytical model described above is justified because the terms of the form  $Pk_x$  and  $Pk_y$  of the 2D  $\mathbf{k} \cdot \mathbf{p}$  Hamiltonian dominate in the expression of the different components of the absorbance. The simple analytical model is justified even more when the energy gap of the semiconductor is small. The deviations from the absorption values predicted by Eq. (18) remain nevertheless small even for large gap materials.

### C. Influence of the SOC on the absorbance

We have seen in Fig. 4 and Fig. 5 that the SOC contributes to bring the plateaus from about  $1.5\pi\alpha$  (at  $E_g$ ) to about  $\pi\alpha$ . Here we discuss the reasons, on the one hand with the help of a simplest-as-possible analytical model describing the main underlying effects, on the other hand by analyzing the results of the tight binding calculations.

#### 1. A prototypical analytical model including SOC

We start from the Kane Hamiltonian [56] including SOC in the basis of Bloch states  $|s \uparrow\rangle, |x \uparrow\rangle, |y \uparrow\rangle, |z \uparrow\rangle, |s \downarrow\rangle, |x \downarrow\rangle, |y \downarrow\rangle, |z \downarrow\rangle$ , where  $Oz$  remains perpendicular to the quantum well. We write the Hamiltonian as two identical  $4 \times$

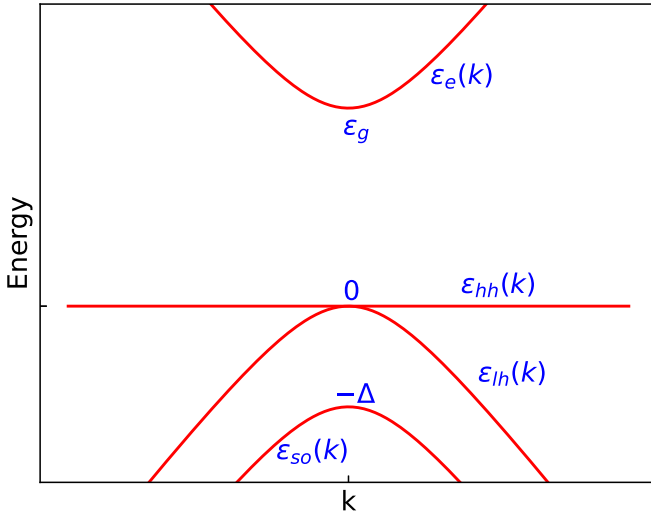


FIG. 6. Band structure in the analytical model including SOC. The energies are noted by the Greek letter  $\varepsilon$  instead of  $E$  to distinguish from the case without SOC.

4 blocks [34]

$$H = \begin{bmatrix} \varepsilon_g & i\sqrt{\frac{2}{3}}Pk & -\frac{i}{\sqrt{3}}Pk & 0 \\ -i\sqrt{\frac{2}{3}}Pk & 0 & 0 & 0 \\ \frac{i}{\sqrt{3}}Pk & 0 & -\Delta & 0 \\ 0 & 0 & 0 & 0 \end{bmatrix} \quad (19)$$

for one block in the basis  $|s \uparrow\rangle, |\frac{3}{2}, \frac{1}{2}\rangle, |\frac{1}{2}, \frac{1}{2}\rangle, |\frac{3}{2}, \frac{3}{2}\rangle$ , for the other one in the basis  $|s \downarrow\rangle, |\frac{3}{2}, -\frac{1}{2}\rangle, |\frac{1}{2}, -\frac{1}{2}\rangle, |\frac{3}{2}, -\frac{3}{2}\rangle$ , eigenvectors of  $\mathbf{J}$  and  $J_z$  with  $Z$  oriented along  $\mathbf{k}$ .  $\varepsilon_g$  is the gap in the presence of SOC, and  $\Delta$  is the splitting between  $J = 3/2$  and  $J = 1/2$  states due to the SOC. The expression of the  $J = 3/2$  and  $J = 1/2$  states in terms of  $|x \uparrow\rangle \dots |z \downarrow\rangle$  is given in Sec. S7 of the Supplemental Material [29].

In the same spirit as before, following Sec. S3 of the Supplemental Material [29], we treat the 2D problem with  $k_z = 0$  ( $k \equiv k_{\parallel}$ ). The corresponding band structure is shown schematically in Fig. 6. The heavy-hole band is flat [ $\varepsilon_{hh}(k) = 0$ ] and is degenerate at  $k = 0$  with the light-hole band [ $\varepsilon_{lh}(k)$ ]. The electron band  $\varepsilon_e(k)$  starts at  $\varepsilon_g$  at  $k = 0$ ; the top of the split-off band  $\varepsilon_{so}(k)$  is at  $-\Delta$ .

Therefore in this model, the absorptance spectrum exhibits two steps, the first one at  $\hbar\omega = \varepsilon_g$  that include two contributions (heavy and light holes  $\rightarrow$  electrons), the second one at  $\hbar\omega = \varepsilon_g + \Delta$  (split-off  $\rightarrow$  electrons). As described in Sec. S7 of the Supplemental Material [29], the height of these steps can be calculated analytically at  $k_{\parallel} = 0$ , the energy dispersions of the different bands being obtained by treating  $Pk$  terms within second order perturbation theory (becomes unvalid when  $\Delta \rightarrow 0$ ). The height of the first and second steps is given by

$$\mathcal{A}_{0,1}(\varepsilon_g) = \pi\alpha \left[ \frac{3}{4\left(1 + \frac{\varepsilon_g}{2(\varepsilon_g + \Delta)}\right)} + \frac{1}{2\left(1 + \frac{\varepsilon_g}{4(\varepsilon_g + \Delta)}\right)} \right] \quad (20)$$

$$\delta\mathcal{A}_{0,2}(\varepsilon_g + \Delta) = \pi\alpha \left[ \frac{1}{2\left(1 + \frac{\varepsilon_g + \Delta}{\varepsilon_g}\right)} \right] \quad (21)$$

where  $\delta\mathcal{A}_{0,2}$  in the second equation means that it must be added to the other contributions at  $\hbar\omega = \varepsilon_g + \Delta$  to get the total absorptance.

Using the data corresponding to the InAs quantum well of 4.2 nm (Fig. 5), i.e.,  $\varepsilon_g \approx 0.7$  eV and  $\Delta \approx 0.4$  eV, the height of the first step [Eq. (20)] is about  $\pi\alpha$ , and the height of the second step [Eq. (21)] is about  $0.2\pi\alpha$ , in excellent agreement with the tight binding results of Fig. 5 and the experimental data of Ref. [13]. Remarkably, Eq. (20) and Eq. (21) only depend on  $x = \varepsilon_g/\Delta$ , and  $\mathcal{A}_0(\varepsilon_g)$  is found to be very close to  $\pi\alpha$  in a wide range of values of  $x$ . Figure S5 of the Supplemental Material [29] shows a deviation of Eq. (20) from  $\pi\alpha$  below 10% for  $x$  between 0.5 and 5. This explains the universality of the  $\pi\alpha$  quantization of the absorptance in the presence of SOC.

## 2. Comparison to tight-binding calculations

Figure 5 allows to understand the effect of the SOC on the absorptance spectrum calculated in tight-binding. The first step found in absence of SOC transforms in three steps. A short plateau at about  $0.7\pi\alpha$  is followed, after a small bump, by a long plateau close to  $\pi\alpha$ . This corresponds to transitions from HH and LH bands, respectively, which were degenerate at  $k_{\parallel} = 0$  by construction in the analytical model. Then, at higher energy ( $\sim 1.1$  eV), there is a third small step (split-off) such that the absorptance finally reaches the value obtained without SOC. Apart from the fact that it does not give a splitting between LH and HH bands, the analytical model accounts for this behavior very well. Note that the respective weights of the steps from HH and LH depend significantly on the nature of the semiconductor, the spin-orbit coupling, and the vertical confinement.

## 3. Summary of our understanding

Figure 7 summarizes our understanding of the origin of absorptance quantization in III-V or II-VI semiconductor quantum wells and in graphene. This quantization comes from the compensation between numerator and denominator in Eq. (4). In the case of graphene, this compensation is exact which leads to an absorptance  $\pi\alpha/2$  for each of the two K valleys.

In the case of a semiconductor quantum well, the situation seems at first sight very different because there are optical transitions between valence bands mainly derived from  $p$  orbitals and a conduction band of strong  $s$  character. However, under strong vertical confinement, in the absence of SOC, the valence band can be described by two bands coupled to the conduction band by terms like  $Pk_x$  and  $Pk_y$ . Transitions between the LH subband and the conduction subband lead to an absorptance of the order of  $\pi\alpha/2$  at the threshold, decreasing to zero at higher energy. Transitions between the HH subband and the conduction subband give a constant absorptance at  $\pi\alpha$ . In the absence of SOC, the total absorptance is thus characterized by a single step at  $\sim 3\pi\alpha/2$  which decreases to  $\pi\alpha$  at higher energy (Fig. 5). This reasoning remains correct as long as  $P^2/E_g$  is large compared to the other terms of the  $\mathbf{k} \cdot \mathbf{p}$  Hamiltonian (Appendix B), which is the situation in many conventional semiconductors [34]. The height of the different contributions of the absorptance can vary from one compound

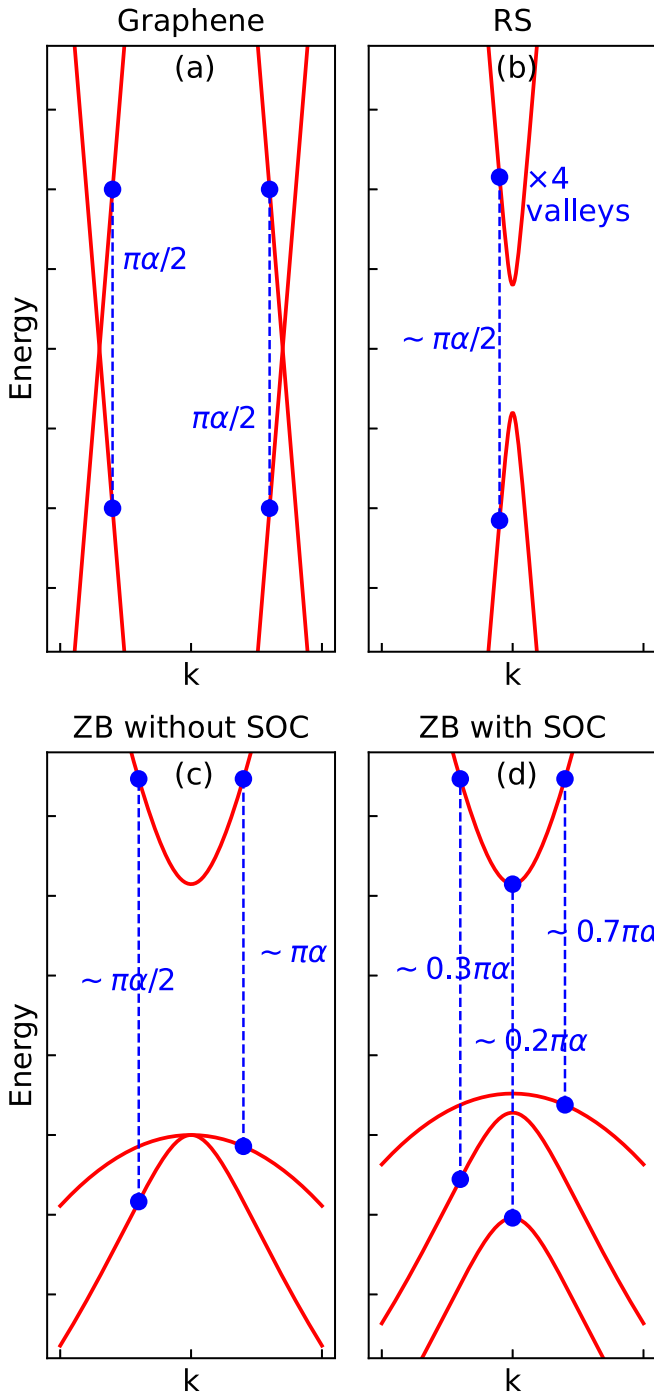


FIG. 7. Schematic representation of electronic bands and optical transitions in graphene (a), in a rocksalt (RS) semiconductor quantum well (b), in a zinc-blende (ZB) semiconductor quantum well without (c) or with (d) SOC. The intensity at the optical thresholds of the absorptance steps is indicated (the values are indicative, they may slightly vary from one material to another). The corresponding data are also summarized in Table I.

to another, but the previous description remains nevertheless qualitatively correct for all the studied zinc-blende materials, especially those with a small band gap.

When the SOC is switched on, the absorptance remains quantized because of the compensation effect due to the dom-

inance of the coupling terms  $Pk_i$ . However, the bands are split and a certain part of the oscillator strength is transferred to the SO band which is lower in energy. This leads to an absorptance  $\approx 0.7\pi\alpha$  for the transitions from HH subband,  $\approx 0.3\pi\alpha$  for those from LH subband, and  $\approx 0.2\pi\alpha$  for those from SO subband [Fig. 7(d)]. The total contribution from transitions from HH and LH subbands is thus close to  $\pi\alpha$ , which explains the wide plateau in Fig. 5. Of course, the  $\pi\alpha$  quantization of the absorptance is not exact, numbers slightly depend on the nature of the semiconductor, the plateaus are not totally flat because the compensation is not perfect, and therefore do not form a standard for the fine structure constant [24]. However, our calculations show that the quantization is universal, provided that excitonic effects can be neglected.

This quantification of the absorptance is visible as long as the energy gap between the  $\pi\alpha$  steps remains smaller than the broadening factors. This gap becomes smaller and smaller as the thickness of the quantum well decreases. In III-V and II-VI materials, this gap is essentially determined by the quantum confinement in the conduction band and thus varies approximately as the inverse of the well thickness square.

## V. REVISITING EXPERIMENTAL DATA ON SUPERLATTICES

The physical effects explaining the quantization of absorptance should be operative also in semiconductor superlattices, provided that the barriers are high and the couplings between quantum wells are weak (multilayers). As already proposed in Ref. [23], this invites us to revisit experimental results obtained on these systems. Typically, the experiments consist of measuring the transmission through relatively thick layers composed of a large number (25–50) of periods, each formed by a quantum well and a barrier. The absorption coefficient  $a(\hbar\omega)$  of the medium, deduced from these measurements, is given quite generally by

$$a(\hbar\omega) = \frac{\omega}{cn} \varepsilon''(\hbar\omega) \quad (22)$$

where  $\varepsilon''$  is the imaginary part of the dielectric constant and  $n$  is the refractive index of the medium. Consequently, the absorptance of a single period can be defined as

$$\mathcal{A}(\hbar\omega) = a(\hbar\omega)L_p \quad (23)$$

where  $L_p = L_w + L_b$  is the length of the period,  $L_w$  ( $L_b$ ) being the thickness of the quantum well (barrier). However, we can deduce from Eq. (22) and the theory that we discussed above, that the quantity of interest, the one to be quantized in units of  $\pi\alpha$ , should be  $n\mathcal{A}(\hbar\omega)$  [23]. In the following, we revisit experimental results from the literature, deliberately presenting them by increasing width of their band gap.

Figure 8 presents the absorptance per period which was measured in  $\text{HgTe}/\text{Hg}_x\text{Cd}_{1-x}\text{Te}$  superlattices. The spectra are characterized by a wide plateau for which  $n\mathcal{A}(\hbar\omega)$  is approximately equal to  $\pi\alpha$ . Just at the optical threshold, there is also a smaller step at approximately  $3\pi\alpha/4$ , which can be attributed to transitions to the heavy-hole subband. Interestingly, the absorptance spectrum that we predicted for a 3.9-nm-thick quantum well of HgTe (Fig. 3) is close to that obtained for  $\text{HgTe}/\text{Hg}_{0.37}\text{Cd}_{0.63}\text{Te}$  superlattices with  $L_w = 3.47$  nm and

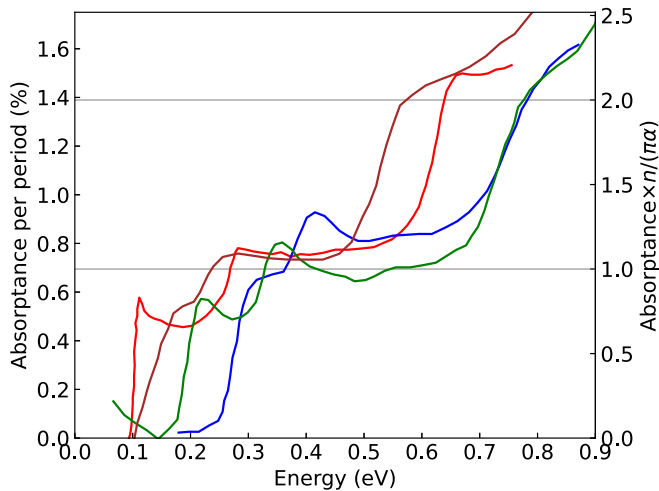


FIG. 8. Absorbance per period in  $\text{HgTe}/\text{Hg}_x\text{Cd}_{1-x}\text{Te}$  superlattices deduced from the measurement of their absorption coefficient (period = well thickness  $L_w$  plus barrier thickness  $L_b$ ). The vertical axis on the right gives the absorbance multiplied by the sample refractive index  $n$  normalized by  $\pi\alpha$ . Red line: data of Ref. [57] for  $x = 0.05$ ,  $L_w = 4.15$  nm,  $L_b = 8.95$  nm. Brown line: data of Ref. [58] for  $x = 0.15$ ,  $L_w = 5.8$  nm,  $L_b = 4.2$  nm. Green line: data of Ref. [59] for  $x = 0.37$ ,  $L_w = 3.47$  nm,  $L_b = 7.60$  nm. Blue line: data of Ref. [60] for  $x = 0.32$ ,  $L_w = 3.4$  nm,  $L_b = 7.70$  nm.

$L_b = 7.60$  nm. However, the experimental spectra exhibit clear bumps at the step edges, which are absent in calculated ones and can be attributed to excitonic effects.

The quantity  $nA(\hbar\omega)$  measured in  $\text{InSb}/\text{Al}_{0.09}\text{In}_{0.91}\text{Sb}$  superlattices at 4.2 K is also characterized by clear steps at  $\pi\alpha$  and  $2\pi\alpha$  (Fig. 9), plus marked peaks which were attributed to excitonic effects [61]. These peaks tend to decrease at higher

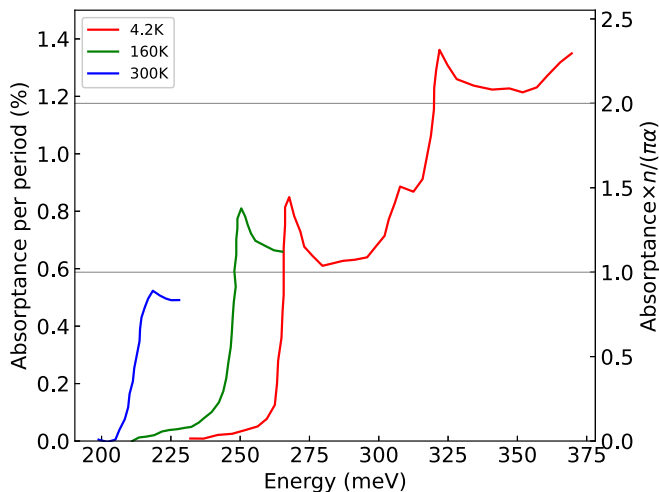


FIG. 9. Absorbance per period in  $\text{InSb}/\text{Al}_{0.09}\text{In}_{0.91}\text{Sb}$  superlattices deduced from the measurement [61] of their absorption coefficient (well thickness = 22.5 nm, barrier thickness = 50 nm) at different temperatures, 4.2 K (red line), 160 K (green line), or 300 K (blue line). The right vertical axis gives the absorbance multiplied by the sample refractive index ( $n = 3.9$ ) normalized by  $\pi\alpha$ . Spectra at 160 K and 300 K were measured in a limited energy range [61].

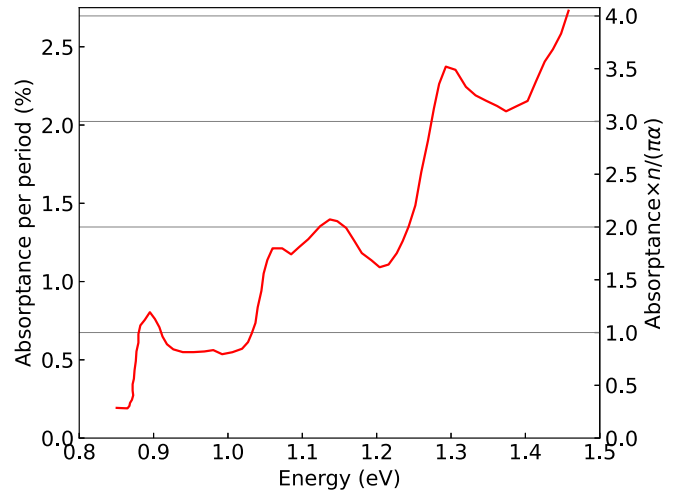


FIG. 10. Absorbance per period in a  $\text{Ga}_{0.47}\text{In}_{0.53}\text{As}/\text{Al}_{0.48}\text{In}_{0.52}\text{As}$  superlattice deduced from the measurement [34] of its absorption coefficient (well thickness = 8.5 nm, barrier thickness = 8.5 nm) at 77K (red line). The right vertical axis gives the absorbance multiplied by the sample refractive index ( $n = 3.4$ ) normalized by  $\pi\alpha$ .

temperature. The  $\pi\alpha$  quantization is also clearly visible in the case of a  $\text{Ga}_{0.47}\text{In}_{0.53}\text{As}/\text{Al}_{0.48}\text{In}_{0.52}\text{As}$  superlattice (Fig. 10), although the excitonic peaks become more prominent.

Figure 11 presents results for  $\text{GaAs}/\text{AlAs}$  superlattices, deduced from measurements made at 2 K [62]. The average value of  $nA(\hbar\omega)$  is clearly above  $\pi\alpha$ . Similar values are obtained in  $\text{GaAs}/\text{AlGaAs}$  (not shown) [63]. These values higher than  $\pi\alpha$  must be seen as a consequence of strong excitonic effects. However,  $\pi\alpha$  remains a good metric of the absorbance.

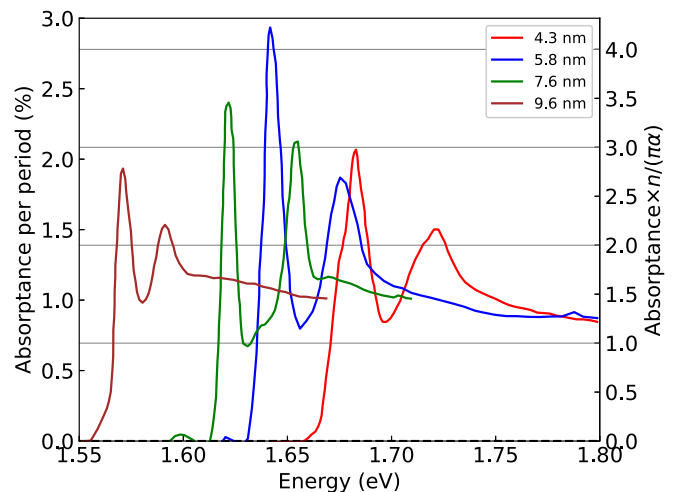


FIG. 11. Absorbance per period in  $\text{GaAs}/\text{AlAs}$  superlattices deduced from the measurement [62] at 2 K of their absorption coefficient (period = well thickness  $L_w$  plus barrier thickness  $L_b$ ). The right vertical axis gives the absorbance multiplied by the sample refractive index  $n$  normalized by  $\pi\alpha$ . Red line:  $L_w = 4.3$  nm,  $L_b = 6.2$  nm. Blue line:  $L_w = 5.8$  nm,  $L_b = 7.1$  nm. Green line:  $L_w = 7.6$  nm,  $L_b = 3.3$  nm. Brown line:  $L_w = 9.6$  nm,  $L_b = 9.1$  nm.

It is important to realize that deviations from  $\pi\alpha$  are expected to be stronger in materials characterized by a wide band gap. On the one hand,  $P^2/E_g$  becomes less dominant compared to the other components of the  $\mathbf{k} \cdot \mathbf{p}$  Hamiltonian [the  $A$ ,  $L$  and  $M$  terms in Eq. (B6) and Eq. (B9) of Appendix B]. Larger deviations are clearly visible in Fig. 3 and Fig. 4. On the other hand, the dielectric constant is lower, the effective masses are usually higher (especially in the conduction and light-hole bands where  $1/m_{e,lh} \propto P^2/E_g$ ), which tends to increase the excitonic effects.

## VI. QUANTUM WELLS OF PbSe

By comparison with InAs and other III-V or II-VI compounds, the case of PbSe (and other IV-VI semiconductors with rocksalt lattice) is interesting since the bulk material is characterized in conduction and valence bands by four nonequivalent valleys at the L point of the Brillouin zone [40]. In the absence of experimental data, we have performed calculations of the absorbance for a 6 nm thick (001) PbSe quantum well. The results, presented in Fig. 12(a), show that  $\mathcal{A}_0(\hbar\omega)$  is also characterized by clear plateaus but of height  $2\pi\alpha$  instead of  $\pi\alpha$ .

Figure 12(b) shows the band structure of the quantum well. Due to the quantum confinement, the energy spectrum is characterized by subbands which are (almost) twofold degenerate, fourfold with spin degeneracy (there is small splitting due to intervalley coupling [40]). In addition, there are two nonequivalent W ( $\pi/a[1, 1, 0]$ ) valleys in the Brillouin zone of the 2D layer. This behavior can be understood by the projection of the four nonequivalent L points ( $\pi/a[1, 1, 1]$ ) of the bulk on the 2D Brillouin zone. The different absorption steps correspond to the transitions allowed only between subbands sharing the same quantum number associated with vertical confinement, i.e.,  $H_i \rightarrow E_i$  [Fig. 12(b)].

Since there are four valleys, absorbance plateaus at  $2\pi\alpha$  mean  $\pi\alpha/2$  contributions from each valley. This behavior is attributed to quasilinear dispersions of the conduction and valence subbands as one moves away from the band gap [Fig. 12(b)], for reasons which are discussed in Ref. [40]. We then find the situation of graphene where the absorbance per valley is  $\pi\alpha/2$ . According to the  $\mathbf{k} \cdot \mathbf{p}$  theory, in each valley, subbands  $H_i$  and  $E_i$  can be described by a  $2 \times 2$  Hamiltonian in which the nondiagonal coupling, of the form  $\mathbf{T} \cdot \mathbf{k}$  where  $\mathbf{T}$  is a 2D vector, becomes dominant when moving away from the edges of the subbands. Our tight-binding calculations thus show that the absorbance quantization in PbSe quantum wells has a physical origin much closer to the case of graphene than to the case of III-V or II-VI semiconductors [Fig. 7(b)].

However, the subbands are parabolic in the vicinity of their edges [Fig. 12(b)]. Consequently, if the broadening  $\eta$  is reduced, the absorbance spectrum develops peaks just above each optical threshold [Fig. 12(a)]. We then recover the situation of tight-binding models on honeycomb lattices in which a band gap is opened under the effect of SOC or an asymmetry between the two sublattices of the honeycomb (see Sec. S8 in the Supplemental Material [29]). The peaks followed by the plateaus reflect the transformation from massive particles to massless particles [26–28].

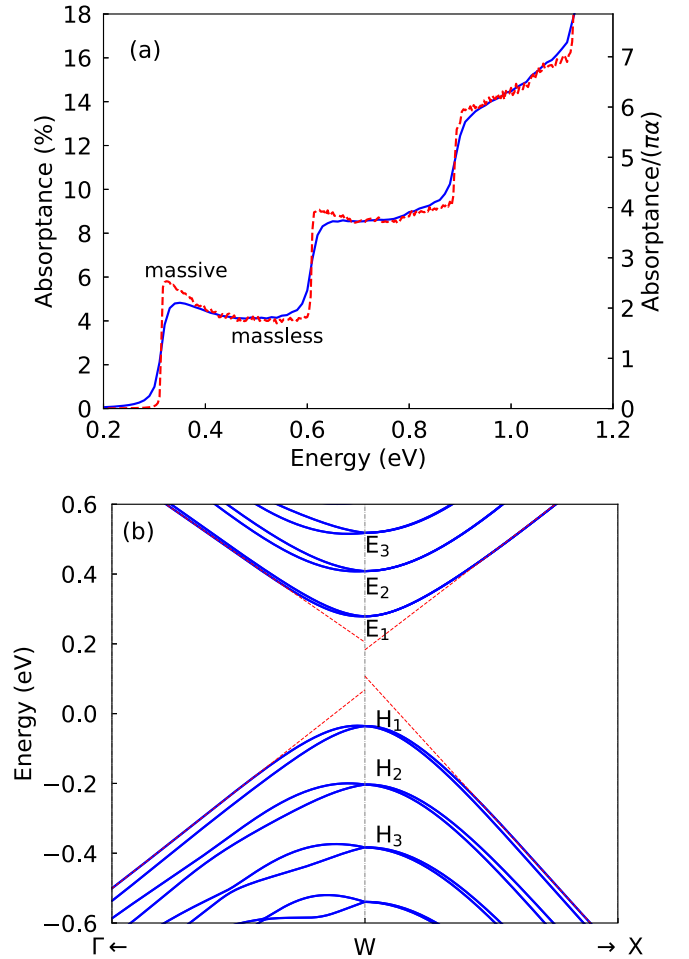


FIG. 12. (a) Bare absorbance  $\mathcal{A}_0(\hbar\omega)$  calculated for a 6 nm thick PbSe quantum wells for two values of the broadening,  $\eta = 10$  meV (blue solid line) or  $\eta = 1$  meV (red dashed line). (b) Zoom on the electron ( $E_i$ ) and hole ( $H_i$ ) subbands in the vicinity of the gap. The red dotted lines show a linear variation of the subbands. The full band structure is presented in Fig. S8, Sec. S9 of Supplemental Material [29].

## VII. CONCLUSION

In conclusion, we have shown that the quantization of the absorbance in semiconductor quantum wells in units of  $\pi\alpha$  is universal. It is predicted for a large number of compounds, provided that the excitonic effects are small. This behavior results from several factors, the main one being the strong coupling of the form  $Pk_x$  and  $Pk_y$ , between conduction and valence subbands. Using a minimum model incorporating only these dominant terms in the Hamiltonian, which nevertheless describes the main underlying physics, the absorbance is found to be directly related to  $\pi\alpha$ , independent of  $P$ , largely independent of the physical quantities characterizing the semiconductor, as in graphene. The SOC also helps bring the absorbance steps closer to integer values of  $\pi\alpha$ , redistributing the oscillator strengths. Experimental results obtained on InAs layers, and on superlattices of other materials, support these conclusions. The situation for IV-VI semiconductors such as PbSe is extremely close to that of graphene in the presence of a band gap. We believe that this work will provide a simplified

view of optical absorption phenomena in 2D or quasi-2D materials for which excitonic effects are not too strong.

## APPENDIX A: ALTERNATIVE EXPRESSION FOR THE ABSORPTANCE

### 1. General case

Using Eq. (3), Eq. (2) can be rewritten in the following form

$$\mathcal{A}_0(\hbar\omega) = \frac{\alpha}{\hbar\omega} \sum_{c,v} \int \frac{|\langle c, \mathbf{k} | \nabla H(\mathbf{k}) | v, \mathbf{k} \rangle|^2}{\delta(\hbar\omega - E_c(\mathbf{k}) + E_v(\mathbf{k})) d^2k} \quad (\text{A1})$$

where we are assuming that, in a cubic semiconductor, the absorptance does not depend on the in-plane orientation of the polarization vector, we can sum the contributions for the two in-plane polarizations and divide by 2 ( $|\langle \nabla H(\mathbf{k}) \cdot \mathbf{x} \rangle|^2 + |\langle \nabla H(\mathbf{k}) \cdot \mathbf{y} \rangle|^2 = |\langle \nabla H(\mathbf{k}) \rangle|^2$ ). For functions  $f$  and  $g$  defined over a  $n$ -dimensional space, we have:

$$\int_{(n)} f(\mathbf{x}) \delta(g(\mathbf{x})) d\mathbf{x} = \int_{(n-1)} \frac{f(\mathbf{x})}{|\nabla g|} d\sigma(\mathbf{x}) \quad (\text{A2})$$

where the second integral is on the  $(n-1)$ -dimensional surface defined by  $g(\mathbf{x}) = 0$ . Equation (A1) can be rewritten as

$$\mathcal{A}_0(\hbar\omega) = \frac{\alpha}{\hbar\omega} \sum_{c,v} \int_{\mathcal{L}_{vc}} \frac{|\langle c, \mathbf{k} | \nabla H(\mathbf{k}) | v, \mathbf{k} \rangle|^2}{|\nabla(E_v(\mathbf{k}) - E_c(\mathbf{k}))|} dl \quad (\text{A3})$$

where  $\mathcal{L}_{vc}$  is the path in  $\mathbf{k}$  space defined by  $\hbar\omega - E_c(\mathbf{k}) + E_v(\mathbf{k}) = 0$ .

### 2. Isotropic case

In the case where all terms only depend on  $k = |\mathbf{k}|$ , Eq. (A3) becomes

$$\mathcal{A}_0(\hbar\omega) = \frac{2\pi\alpha k}{\hbar\omega} \sum_{c,v} \frac{|\langle c, \mathbf{k} | \nabla H(\mathbf{k}) | v, \mathbf{k} \rangle|^2}{\partial|E_v(k) - E_c(k)|/\partial k} \quad (\text{A4})$$

with  $k$  such that  $E_c(k) - E_v(k) = \hbar\omega$ . This expression can be rewritten in another form given in Eq. (4).

The JDOS per unit area can be calculated in a similar way. For the pair of bands  $v$  and  $c$ , the JDOS is

$$J_{c,v}(\hbar\omega) = \frac{1}{S} \sum_{\mathbf{k}} \delta(\hbar\omega - E_c(\mathbf{k}) + E_v(\mathbf{k})) \quad (\text{A5})$$

which, in the isotropic case, transforms into

$$J_{c,v}(\hbar\omega) = \frac{1}{\pi} \frac{k}{\partial|E_c(k) - E_v(k)|/\partial k}. \quad (\text{A6})$$

The bare absorptance can be written as

$$\mathcal{A}_0(\hbar\omega) = \frac{2\pi^2\alpha}{\hbar\omega} \sum_{c,v} J_{c,v}(\hbar\omega) |\langle c, \mathbf{k} | \nabla H(\mathbf{k}) | v, \mathbf{k} \rangle|^2 \quad (\text{A7})$$

with  $k$  such that  $E_c(k) - E_v(k) = \hbar\omega$ .  $|\langle c, \mathbf{k} | \nabla H(\mathbf{k}) | v, \mathbf{k} \rangle|^2 / (\hbar\omega)$  is related to the oscillator strength.

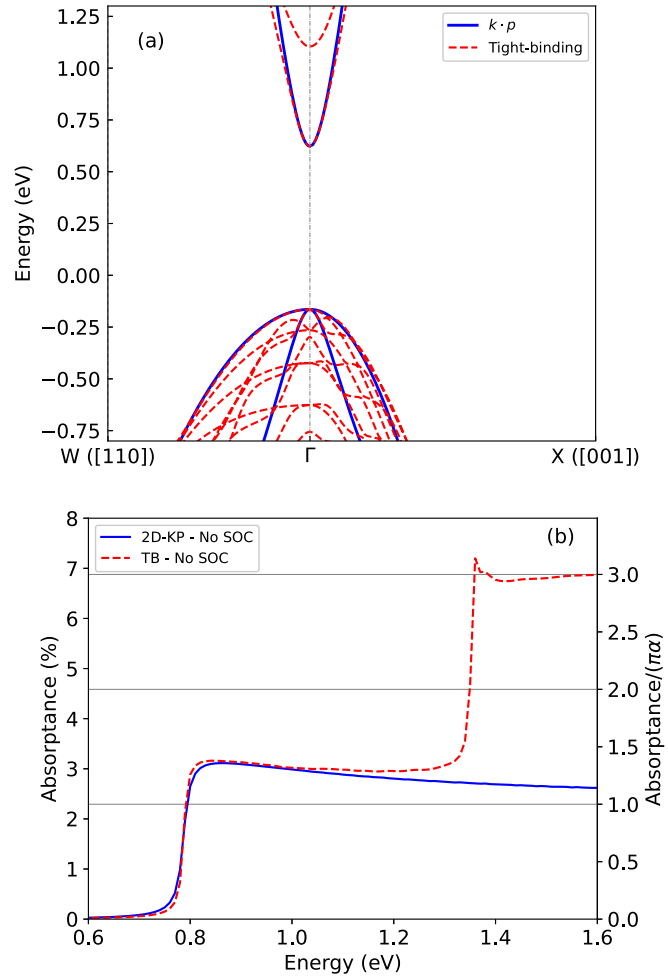


FIG. 13. Comparison between tight-binding (red dashed lines) and 2D  $\mathbf{k} \cdot \mathbf{p}$  (blue solid lines) calculations for 4.2-nm-thick InAs quantum well. SOC is not included. (a) Band structure. (b) Bare absorptance  $\mathcal{A}_0(\hbar\omega)$ .

## APPENDIX B: 2D $\mathbf{k} \cdot \mathbf{p}$ MODEL DEDUCED FROM TIGHT BINDING

Section S3 of the Supplemental Material [29] gives the rationale for describing, in quantum wells, the bands in the vicinity of the band gap with a 2D  $\mathbf{k} \cdot \mathbf{p}$  model. Here we describe how we deduce a  $\mathbf{k} \cdot \mathbf{p}$  Hamiltonian directly from tight binding calculations, without adjusting any parameters. We also present calculations of the absorptance in this model, to go beyond the approximations made in the analytic model of Sec. IV B.

### 1. Derivation of the 2D model

We consider a InAs quantum well of thickness 4.2 nm, chosen because it is characterized by two symmetric surfaces. The system is thus characterized by a perfect in-plane square symmetry, which simplifies the derivation of a 2D  $\mathbf{k} \cdot \mathbf{p}$  model. Figure 13 shows that the band structure calculated without SOC is again characterized by many subbands, with complex dispersion in the valence band. However, the absorptance spectrum exhibits a simple behavior (Fig. 5). The analysis

of the optical matrix elements shows that the first plateau corresponds to transitions from the two highest valence bands (heavy hole and light hole), degenerate at  $k_{\parallel} = 0$ , to the lowest conduction subband (Fig. S6 of the Supplemental Material [29]).

Next, we deduce a  $3 \times 3$   $\mathbf{k} \cdot \mathbf{p}$  matrix using the calculation of the first-order and second-order derivatives of the tight-binding Hamiltonian matrix with respect to  $k_x$  and  $k_y$ , restricted to the lowest conduction subband and the two highest valence subbands, but renormalizing the  $\mathbf{k} \cdot \mathbf{p}$  parameters to include the effects of the remote bands (see Sec. S5 of the Supplemental Material [29] for the methodology). We obtain

$$\tilde{H} = \begin{bmatrix} E_c + Ak^2 & iPk_x & iPk_y \\ -iPk_x & E_v + Lk_x^2 + Mk_y^2 & Nk_x k_y \\ -iPk_y & Nk_x k_y & E_v + Lk_y^2 + Mk_x^2 \end{bmatrix} \quad (\text{B1})$$

in the basis of the three vectors  $|s\rangle$ ,  $|x\rangle$ , and  $|y\rangle$ . The parameters directly derived from the tight-binding Hamiltonian are given by (in atomic units):  $A = 0.00242$ ,  $P = 0.52684$ ,  $E_c = 0.02288$ ,  $E_v = -0.00604$ ,  $L = 2.78493$ ,  $M = -0.81699$ ,  $N = 2.71777$ .  $E_c$  and  $E_v$  differ from the bulk values, since they include the effect of the confinement along  $z$  ( $E_v = 0$  in the bulk).

Figure 13 presents the comparison between tight-binding and 2D  $\mathbf{k} \cdot \mathbf{p}$  band structures and the comparison between absorptance spectra. In spite of its apparent simplicity, since it only describes two valence subbands of the quantum well, the 2D  $\mathbf{k} \cdot \mathbf{p}$  model gives a perfect description of the first step of  $\mathcal{A}_0(\hbar\omega)$ .

## 2. Simplified 2D $\mathbf{k} \cdot \mathbf{p}$ isotropic model

In order to obtain analytical expressions for the absorptance, it is useful to derive a simpler 2D  $\mathbf{k} \cdot \mathbf{p}$  isotropic model. We use the two vectors  $|p_{\parallel}\rangle$  and  $|p_{\perp}\rangle$  previously defined [Eq. (9)].

The Hamiltonian matrix element  $\langle p_{\parallel} | H | p_{\perp} \rangle$  vanishes when  $N = L - M$ . In the bulk, this takes place when the Luttinger parameters  $\gamma_2^I$  and  $\gamma_3^I$  are equal, which corresponds to the spherical symmetry [64]. In this condition, the Hamiltonian written in  $|s\rangle$ ,  $|p_{\parallel}\rangle$ , and  $|p_{\perp}\rangle$  is simply given by:

$$H = \begin{bmatrix} E_s(k) & iPk & 0 \\ -iPk & E_{\parallel}(k) & 0 \\ 0 & 0 & E_{\perp}(k) \end{bmatrix} \quad (\text{B2})$$

with

$$E_s(k) = E_c + Ak^2 \quad E_{\parallel}(k) = E_v + Lk^2 \quad E_{\perp}(k) = E_v + Mk^2. \quad (\text{B3})$$

The solutions are  $|\Psi_{hh}\rangle = |p_{\perp}\rangle$ ,  $|\Psi_e\rangle$ ,  $|\Psi_{lh}\rangle$  of energy  $E_{hh}(k)$  and

$$E_{lh}(k) = \left( \frac{E_s(k) + E_{\parallel}(k)}{2} \right) \pm \sqrt{\left( \frac{E_s(k) - E_{\parallel}(k)}{2} \right)^2 + P^2 k^2}, \quad (\text{B4})$$

respectively.  $E_e(k)$  is the energy of the conduction subband.  $E_{hh}(k)$  and  $E_{lh}(k)$  are the energies of the heavy and light hole subbands, respectively.

## 3. Calculation of the absorptance

The absorptance  $\mathcal{A}_0(\hbar\omega) = \mathcal{A}_{hh-e}(\hbar\omega) + \mathcal{A}_{lh-e}(\hbar\omega)$  is calculated analytically using Eq. (A4) of Appendix A. In this isotropic approximation, we use the previous parameters for the 2D  $\mathbf{k} \cdot \mathbf{p}$  model except that we set  $N = L - M$ . After some algebra (Sec. S6 of the Supplemental Material [29]), the different terms can be calculated to the second order in  $k$  as

$$\mathcal{A}_{hh-e}(\hbar\omega) = \pi\alpha(C_0 + C_2 k^2) + O(k^3) \quad (\text{B5})$$

$$C_0 = \frac{P^2}{(AE_g - E_g M + P^2)} \quad (\text{B6})$$

$$C_2 = -\frac{U}{E_g(A - M + U)^2} \times (A^2 + 2AL - 4AM + AU - 2LM + 4LU + 3M^2 - 5MU) \quad (\text{B7})$$

with  $U = P^2/E_g$  and  $k$  is solution of  $E_e(k) - E_{hh}(k) = \hbar\omega$ . Similarly, we obtain

$$\mathcal{A}_{lh-e}(\hbar\omega) = \pi\alpha(D_0 + D_2 k^2) + O(k^3) \quad (\text{B8})$$

$$D_0 = \frac{P^2}{AE_g - E_g L + 2P^2} \quad (\text{B9})$$

$$D_2 = -\frac{U(5A^2 - 10AL + 12AU + 5L^2 - 12LU + 8U^2)}{E_g(A - L + 2U)^2} \quad (\text{B10})$$

in which  $k$  is solution of  $E_e(k) - E_{lh}(k) = \hbar\omega$ .

With the parameters given above for the 4.2-nm-thick InAs quantum well,  $C_0 = 0.92$ , which is close to 1 because  $P^2/E_g \gg A - M$ . Numerical evaluations show that the variation with  $k$  and with  $\hbar\omega$  is weak (Fig. S4 of the Supplemental Material [29]), i.e.,  $C_2 k^2 \ll C_0$ . It means that  $\mathcal{A}_{hh-e}(\hbar\omega)$  is very close to  $\pi\alpha$  but smaller. With the same parameters,  $D_0 = 0.58$  is close to  $1/2$ , because the term  $2P^2$  is dominant in the denominator of Eq. (B9).  $\mathcal{A}_{lh-e}(\hbar\omega)$  is equal to  $0.58\pi\alpha$  at the energy gap but it decreases at higher energy as  $D_2 k^2$  becomes non-negligible compared to  $D_0$ .

We conclude that the 2D  $\mathbf{k} \cdot \mathbf{p}$  model and its simplified version under isotropic approximation explain very well the absorptance spectrum calculated in tight binding in the absence of SOC. This also completely justifies the simple analytical model of Sec. IV B in which  $A, L, M, N = 0$ . An additional discussion of compensation mechanisms leading to absorptance quantization is presented in Sec. S6.4 of the Supplemental Material [29].

- [1] A. Sommerfeld, The quantum theory of spectral lines, *Ann. Phys.* **356**, 1 (1916).
- [2] R. Feynman, *QED: The Strange Theory of Light and Matter*, Alix G. Mautner memorial lectures (Princeton University Press, Princeton, NJ, 2006).
- [3] J. Maciejko, X.-L. Qi, H. D. Drew, and S.-C. Zhang, Topological Quantization in Units of the Fine Structure Constant, *Phys. Rev. Lett.* **105**, 166803 (2010).
- [4] K. v. Klitzing, G. Dorda, and M. Pepper, New Method for High-Accuracy Determination of the Fine-Structure Constant Based on Quantized Hall Resistance, *Phys. Rev. Lett.* **45**, 494 (1980).
- [5] V. P. Gusynin, S. G. Sharapov, and J. P. Carbotte, Unusual Microwave Response of Dirac Quasiparticles in Graphene, *Phys. Rev. Lett.* **96**, 256802 (2006).
- [6] N. M. R. Peres, F. Guinea, and A. H. Castro Neto, Electronic properties of disordered two-dimensional carbon, *Phys. Rev. B* **73**, 125411 (2006).
- [7] L. A. Falkovsky and A. A. Varlamov, Space-time dispersion of graphene conductivity, *Eur. Phys. J. B* **56**, 281 (2007).
- [8] R. R. Nair, P. Blake, A. N. Grigorenko, K. S. Novoselov, T. J. Booth, T. Stauber, N. M. R. Peres, and A. K. Geim, Fine structure constant defines visual transparency of graphene, *Science* **320**, 1308 (2008).
- [9] K. F. Mak, M. Y. Sfeir, Y. Wu, C. H. Lui, J. A. Misewich, and T. F. Heinz, Measurement of the Optical Conductivity of Graphene, *Phys. Rev. Lett.* **101**, 196405 (2008).
- [10] K. F. Mak, L. Ju, F. Wang, and T. F. Heinz, Optical spectroscopy of graphene: From the far infrared to the ultraviolet, *Solid State Commun.* **152**, 1341 (2012).
- [11] G. Zhang, S. Huang, F. Wang, Q. Xing, C. Song, C. Wang, Y. Lei, M. Huang, and H. Yan, The optical conductivity of few-layer black phosphorus by infrared spectroscopy, *Nat. Commun.* **11**, 1847 (2020).
- [12] V. G. Kravets, F. Schedin, and A. N. Grigorenko, Fine structure constant and quantized optical transparency of plasmonic nanoarrays, *Nat. Commun.* **3**, 640 (2012).
- [13] H. Fang, H. A. Bechtel, E. Plis, M. C. Martin, S. Krishna, E. Yablonovitch, and A. Javey, Quantum of optical absorption in two-dimensional semiconductors, *Proc. Natl. Acad. Sci. USA* **110**, 11688 (2013).
- [14] K. F. Mak, C. Lee, J. Hone, J. Shan, and T. F. Heinz, Atomically Thin MoS<sub>2</sub>: A New Direct-Gap Semiconductor, *Phys. Rev. Lett.* **105**, 136805 (2010).
- [15] M. Bernardi, M. Palummo, and J. C. Grossman, Extraordinary sunlight absorption and one nanometer thick photovoltaics using two-dimensional monolayer materials, *Nano Lett.* **13**, 3664 (2013).
- [16] L. Britnell, R. M. Ribeiro, A. Eckmann, R. Jalil, B. D. Belle, A. Mishchenko, Y.-J. Kim, R. V. Gorbachev, T. Georgiou, S. V. Morozov, A. N. Grigorenko, A. K. Geim, C. Casiraghi, A. H. C. Neto, and K. S. Novoselov, Strong light-matter interactions in heterostructures of atomically thin films, *Science* **340**, 1311 (2013).
- [17] K. He, N. Kumar, L. Zhao, Z. Wang, K. F. Mak, H. Zhao, and J. Shan, Tightly Bound Excitons In Monolayer WSe<sub>2</sub>, *Phys. Rev. Lett.* **113**, 026803 (2014).
- [18] Y. Li, A. Chernikov, X. Zhang, A. Rigosi, H. M. Hill, A. M. van der Zande, D. A. Chenet, E.-M. Shih, J. Hone, and T. F. Heinz, Measurement of the optical dielectric function of monolayer transition-metal dichalcogenides: MoS<sub>2</sub>, MoSe<sub>2</sub>, Ws<sub>2</sub>, and WSe<sub>2</sub>, *Phys. Rev. B* **90**, 205422 (2014).
- [19] G. Wang, A. Chernikov, M. M. Glazov, T. F. Heinz, X. Marie, T. Amand, and B. Urbaszek, Colloquium: Excitons in atomically thin transition metal dichalcogenides, *Rev. Mod. Phys.* **90**, 021001 (2018).
- [20] S. Ithurria, M. D. Tessier, B. Mahler, R. P. S. M. Lobo, B. Dubertret, and A. L. Efros, Colloidal nanoplatelets with two-dimensional electronic structure, *Nat. Mater.* **10**, 936 (2011).
- [21] Z. Chen, B. Nadal, B. Mahler, H. Aubin, and B. Dubertret, Quasi-2D colloidal semiconductor nanoplatelets for narrow electroluminescence, *Adv. Funct. Mater.* **24**, 295 (2014).
- [22] T. Stauber, N. M. R. Peres, and A. K. Geim, Optical conductivity of graphene in the visible region of the spectrum, *Phys. Rev. B* **78**, 085432 (2008).
- [23] T. Szkopek, Optical frequency conductance, susceptance and admittance of quantum wells, *IEEE J. Quantum Electron.* **47**, 500 (2011).
- [24] M. Yoshita, K. Kamide, H. Suzuura, and H. Akiyama, Applicability of continuum absorption in semiconductor quantum wells to absolute absorption-strength standards, *Appl. Phys. Lett.* **101**, 032108 (2012).
- [25] L. Matthes, O. Pulci, and F. Bechstedt, Massive dirac quasiparticles in the optical absorbance of graphene, silicene, germanene, and tinene, *J. Phys.: Condens. Matter* **25**, 395305 (2013).
- [26] T. Stauber, D. Noriega-Pérez, and J. Schliemann, Universal absorption of two-dimensional systems, *Phys. Rev. B* **91**, 115407 (2015).
- [27] D. J. Merthe and V. V. Kresin, Transparency of graphene and other direct-gap two-dimensional materials, *Phys. Rev. B* **94**, 205439 (2016).
- [28] R. Huang, J. Li, Z. Wu, W. Yang, W. Huang, C. Li, and S. Chen, Universal absorption of two-dimensional materials within k.p method, *Phys. Lett. A* **382**, 3035 (2018).
- [29] See Supplemental Material at <http://link.aps.org/supplemental/10.1103/PhysRevB.105.035421> for additional results on InAs, HgTe, PbSe, PbS quantum wells, on the justification and the derivation of the 2D  $\mathbf{k} \cdot \mathbf{p}$  model, on detailed derivations of the analytical models, on calculations of the absorptance in tight-binding models on honeycomb lattices.
- [30] G. Fishman, *Semi-conducteurs: Les bases de la théorie K.P* (Editions de l'Ecole Polytechnique, Palaiseau, 2010).
- [31] P. R. Wallace, The band theory of graphite, *Phys. Rev.* **71**, 622 (1947).
- [32] C. L. Kane and E. J. Mele, Quantum Spin Hall Effect in Graphene, *Phys. Rev. Lett.* **95**, 226801 (2005).
- [33] T. G. Pedersen, Analytic calculation of the optical properties of graphite, *Phys. Rev. B* **67**, 113106 (2003).
- [34] G. Bastard, *Wave Mechanics Applied to Semiconductor Heterostructures* (Les Editions de Physique, Les Ulis, France, 1990).
- [35] H. A. Washburn, J. R. Sites, and H. H. Wieder, Electronic profile of *n*-inas on semi-insulating gaas, *J. Appl. Phys.* **50**, 4872 (1979).
- [36] I. Vurgaftman, J. R. Meyer, and L. R. Ram-Mohan, Band parameters for iii-v compound semiconductors and their alloys, *J. Appl. Phys.* **89**, 5815 (2001).
- [37] G. Mugny, D. Rideau, F. Triozon, Y.-M. Niquet, C. Kriso, F. Pereira, D. Garetto, C. Tavernier, and C. Delerue, Full-zone

- k. p parametrization for iii-as materials, in *2015 International Conference on Simulation of Semiconductor Processes and Devices (SISPAD)* (2015), pp. 28–31.
- [38] C. Delerue and M. Lannoo, *Nanostructures: Theory and Modeling* (Springer, Berlin, 2004).
- [39] M. Dressel and G. Grüner, in *Electrodynamics of Solids: Optical Properties of Electrons in Matter* (Cambridge University Press, Cambridge, 2002).
- [40] G. Allan and C. Delerue, Confinement effects in pbse quantum wells and nanocrystals, *Phys. Rev. B* **70**, 245321 (2004).
- [41] T. B. Boykin, G. Klimeck, R. C. Bowen, and F. Oyafuso, Diagonal parameter shifts due to nearest-neighbor displacements in empirical tight-binding theory, *Phys. Rev. B* **66**, 125207 (2002).
- [42] M. Dufour, E. Izquierdo, C. Livache, B. Martinez, M. G. Silly, T. Pons, E. Lhuillier, C. Delerue, and S. Ithurria, Doping as a strategy to tune color of 2D colloidal nanoplatelets, *ACS Appl. Mater. Interfaces* **11**, 10128 (2019).
- [43] Y. Tan, M. Povolotskyi, T. Kubis, Y. He, Z. Jiang, G. Klimeck, and T. B. Boykin, Empirical tight binding parameters for gaas and mgo with explicit basis through DFT mapping, *J. Comput. Electron.* **12**, 56 (2013).
- [44] T. B. Boykin, G. Klimeck, and F. Oyafuso, Valence band effective-mass expressions in the  $sp^3d^5s^*$  empirical tight-binding model applied to a Si and Ge parametrization, *Phys. Rev. B* **69**, 115201 (2004).
- [45] G. Allan and C. Delerue, Tight-binding calculations of the optical properties of HgTe nanocrystals, *Phys. Rev. B* **86**, 165437 (2012).
- [46] A. N. Poddubny, M. O. Nestoklon, and S. V. Goupalov, Anomalous suppression of valley splittings in lead salt nanocrystals without inversion center, *Phys. Rev. B* **86**, 035324 (2012).
- [47] Y. M. Niquet, D. Rideau, C. Tavernier, H. Jaouen, and X. Blase, Onsite matrix elements of the tight-binding hamiltonian of a strained crystal: Application to silicon, germanium, and their alloys, *Phys. Rev. B* **79**, 245201 (2009).
- [48] M. Graf and P. Vogl, Electromagnetic fields and dielectric response in empirical tight-binding theory, *Phys. Rev. B* **51**, 4940 (1995).
- [49] D. Petrovykh, M. Yang, and L. Whitman, Chemical and electronic properties of sulfur-passivated InAs surfaces, *Surf. Sci.* **523**, 231 (2003).
- [50] M. L. Cohen and T. K. Bergstresser, Band structures and pseudopotential form factors for fourteen semiconductors of the diamond and zinc-blende structures, *Phys. Rev.* **141**, 789 (1966).
- [51] S. Murakami, N. Nagaosa, and S.-C. Zhang, Spin-Hall Insulator, *Phys. Rev. Lett.* **93**, 156804 (2004).
- [52] B. A. Bernevig, T. L. Hughes, and S.-C. Zhang, Quantum spin hall effect and topological phase transition in HgTe quantum wells, *Science* **314**, 1757 (2006).
- [53] M. König, S. Wiedmann, C. Brüne, A. Roth, H. Buhmann, L. W. Molenkamp, X.-L. Qi, and S.-C. Zhang, Quantum spin hall insulator state in HgTe quantum wells, *Science* **318**, 766 (2007).
- [54] E. Izquierdo, A. Robin, S. Keuleyan, N. Lequeux, E. Lhuillier, and S. Ithurria, Strongly confined hgte 2D nanoplatelets as narrow near-infrared emitters, *J. Am. Chem. Soc.* **138**, 10496 (2016).
- [55] A. H. Castro Neto, F. Guinea, N. M. R. Peres, K. S. Novoselov, and A. K. Geim, The electronic properties of graphene, *Rev. Mod. Phys.* **81**, 109 (2009).
- [56] E. Kane, Energy band structure in P-type germanium and silicon, *J. Phys. Chem. Solids* **1**, 82 (1956).
- [57] C. R. Becker, V. Latussek, A. Pfeuffer-Jeschke, G. Landwehr, and L. W. Molenkamp, Band structure and its temperature dependence for type-iii HgTe/Hg<sub>1-x</sub>Cd<sub>x</sub>Te superlattices and their semimetal constituent, *Phys. Rev. B* **62**, 10353 (2000).
- [58] Y. Lansari, J. W. Han, S. Hwang, L. S. Kim, J. W. Cook, J. F. Schetzina, J. N. Schulman, and N. Otsuka, Properties of HgTe–Hg<sub>0.15</sub>Cd<sub>0.85</sub>Te superlattices grown by molecular-beam epitaxy, *J. Vac. Sci. Technol. B* **7**, 241 (1989).
- [59] C. R. Becker, V. Latussek, H. Heinke, M. M. Regnet, F. Goschenhofer, S. Einfeldt, L. He, E. Bangert, M. M. Kraus, and G. Landwehr, Molecular beam epitaxial growth and characterization of (001) Hg<sub>1-x</sub>Cd<sub>x</sub>Te–HgTe superlattices, in *Growth and Characterization of Materials for Infrared Detectors*, Vol. 2021, edited by R. E. Longshore and J. W. Baars, International Society for Optics and Photonics (SPIE, 1993), pp. 138–148.
- [60] C. R. Becker, V. Latussek, W. Spahn, F. Goschenhofer, S. Oehling, and G. Landwehr, Molecular beam epitaxial growth and optical properties of (001) HgTe/Hg<sub>1-x</sub>Cd<sub>x</sub>Te superlattices, in *Growth and Characterization of Materials for Infrared Detectors II*, Vol. 2554, edited by R. E. Longshore, J. W. Baars, A. Kepten, and J. M. Trombetta, International Society for Optics and Photonics (SPIE, 1995), pp. 6–14.
- [61] N. Dai, F. Brown, R. E. Doezema, S. J. Chung, and M. B. Santos, Temperature dependence of exciton linewidths in InSb quantum wells, *Phys. Rev. B* **63**, 115321 (2001).
- [62] Y. Masumoto, M. Matsuura, S. Tarucha, and H. Okamoto, Direct experimental observation of two-dimensional shrinkage of the exciton wave function in quantum wells, *Phys. Rev. B* **32**, 4275 (1985).
- [63] W. T. Masselink, P. J. Pearah, J. Klem, C. K. Peng, H. Morkoç, G. D. Sanders, and Y.-C. Chang, Absorption coefficients and exciton oscillator strengths in AlGaAs–GaAs superlattices, *Phys. Rev. B* **32**, 8027 (1985).
- [64] A. Baldereschi and N. O. Lipari, Spherical model of shallow acceptor states in semiconductors, *Phys. Rev. B* **8**, 2697 (1973).